Measurement of Developing Turbulent Flow in a U-Bend of Circular Cross-Section

Gun Hyee Lee
Department of Mechanical Engineering, Wonkwang University, Shinyoungdong, Iksan, Chullabukdo, 570-49, Korea
Young Don Choi*
Department of Mechanical Engineering, Korea University, Anamdong, Sungpukku, Seoul 136-701, Korea
Seong Ho Han
Department of Mechanical Engineering, Korea University, Anamdong, Sungpukku, Seoul 136-701, Korea

Hot-wire measurements of the full mapping of the velocity and Reynolds stress components are reported for developing turbulent flow in a strongly curved 180 deg pipe and its tangents. A slanted wire is rotated into 6 orientations and the voltage outputs from wires are combined to obtain the mean velocity and Reynolds stress components. The strength of secondary flow reaches up to the 28% of bulk mean velocity. The strong counter-rotating vortex pair induced by the transverse pressure gradient and centrifugal force imbalance grows up to $\theta=67.5°$into the bend. But the vortex pair breaks down into two cell pattern after $\theta=90°$ Core vortex formation and reversal of secondary flow direction along the bend symmetry plane is cleanly found in the secondary vector plot. At $\theta=67.5°$ and $\theta=90°$ into bend a large "trough" develops in the longitudinal velocity toward the inside of the bend due to the breakdown of secondary flow. In the bend, the mean longitudinal velocity component changes little after $\theta=90°$, but secondary flow never achieves fully-developed state. Similar behaviors are observed in the radial and circumferential stresses.

Key Words : Transonic/Supersonic Flows, Air Jet Loom, Backward Facing Step, Unsteady Flow, Recirculating Flow

Nomenclature

D : Diameter of pipe
D_n : Dean number $=\mathrm{Re}(D/R_C)^{1/2}$
E : Instantaneous voltage of hot-wire
e : Fluctuating voltage of hot-wire
k_{θ_i} : Coefficient of hot-wire orientatation
$K_{E_iE_j}$: Covariance between wires i and j
K_S : Coefficient of hot-wire characteristics
R_C : Radius of duct curvature
Re : Reynolds number $(=W_BD_H/v)$
u : Circumferential fluctuating velocity
U : Circumferential mean velocity component
U_e : Effective velocity
$\bar{u}_i\bar{u}_j$: Reynolds stress tensor
V : Radial mean velocity component
v : Radial fluctuating velocity
V_λ : Resultant velocity vector
W : Stream-wise mean velocity component
W_B : Stream-wise bulk velocity
w : Stream-wise fluctuating velocity
X : Stream-wise coordinate
$\bar{X}_\theta$: Mean effective velocity
r : Radial coordinate

* Corresponding Author,
E-mail : ydchoi@korea.ac.kr
TEL : +82-2-3290-3355; **FAX** : +82-2-928-1067
Department of Mechanical Engineering, Korea University, Anamdong, Sungpukku, Seoul 136-701, Korea.
(Manuscript **Received** August 14, 2006; **Revised** December 9, 2006)

$\gamma_{E_iE_J}$: Correlation coefficient between cooling velocities of adjacent wire orientations
θ : Rotation angle of hot-wire, bend angle from entrance
κ : Experimental constant
ν : Kinetic viscosity
ξ : Angle between V_λ and a wire
ρ : Density
σ^2 : Variance of a given quantity
φ : Circumferential angle from outer most radius of bend curvature, circumferential coordinate

Subscripts

l, m : Dummy indices which take the valves 1 to 3
1, 2, 3, 4, 5, 6 : Refers to the six probe measuring positions
θ : Rotation angle of hot-wire, bend angle

1. Introduction

Turbulent flows in a curved duct are widely encountered in the mechanical equipments and systems, for example, in the flow passages between turbine and compressor, pipe bends in heat exchangers, cooling passages inside gas turbine blade, and blood vessels. In a curved duct, radial pressure gradients push the slowly moving fluid near the side walls toward the convex wall while the fluid near the plane of duct symmetry toward the concave wall. This viscous-inviscid mechanism creates secondary flow. The secondary flow can be of the order of 10~40% of the mean streamwise velocity (Johnson, 1984). For twenty years, a large amount of measurements have been conducted for the developing turbulent flows in the curved ducts of square cross-section (Humphrey, 1981; Taylor et al., 1982; Chang et al., 1983; Choi et al., 1990). However, the measurements of turbulent flow field in the curved pipes appear to be relatively sparse, although the information on the flow fields in the curved pipes are more important in practice. It is partly due to the greater difficulties associated with the experimental method (Azzola et al., 1986).

Rowe (1970) obtained the total pressure and yaw results for the turbulent flow in a 180 deg bend and the attached downstream tangents. In Rowe's experiment $Rc/D=12$ and Re=236,000, where Rc is the bend mean radius of curvature, D its diameter and Re is the Reynolds number based on the bulk mean velocity. Rowe reported that the secondary flow is most intense at about 30 deg into bend. Near this position, the total pressure gradient induces a stream-wise component of vorticity opposite in sense of rotation to the stream-wise vorticity produced at the entrance of the bend. Rowe also reported that the curved pipe flow is essentially fully developed past $\theta=90$ deg. There is evidence of local reversal in the secondary flow direction along the bend symmetry plane between $\theta=90$ deg and $X/D=+5$. But Rowe's experimental results were uncertain because of the effect of the mechanical probe used in the measurement on the flow field could not be removed. Azzola et al.(1986) investigated the developing turbulent flow in a strongly curved 180 deg pipe and its downstream tangents both experimentally and by the numerical simulation. They measured the longitudinal and circumferential velocity components and three Reynolds stress components by Laser-Doppler anemometer. In their simulation, k-ε eddy viscosity model was used. Since their LDV measurements were restricted to vertical (radial) scan in the surface $\varphi=\pi/2$ in the symmetrical upper half of the test section, a full mapping of the velocity fields and Reynolds stress distributions over the entire flow regions could not be obtained. Choi et al.(1997) reported fine grid calculations for the Azzola et al.'s (1986) flow conditions using both k-ε eddy viscosity model and algebraic second moment closure. Choi et al.'s simulation using second moment closure gave much improved results for mean velocities, and turbulent intensities in compared with k-ε eddy viscosity model.

In the present study, hot-wire measurements of the full mapping of the velocity and Reynolds stress components are performed for developing turbulent flow in a strongly curved 180 deg pipe and its tangents. A slanted wire is rotated into 6 orientations and the voltage outputs from wires are combined to obtain the mean velocity and

Reynolds stress components.

2. Experiment

2.1 Experimental apparatus and methodology

The basic components of the test section are shown schematically in Fig. 1. They comprised two straight pipes and a 180 deg curved pipe, constructed from transparent plexiglass. The pipe cross-section is circular throughout with 88.9± 0.4 mm inner diameter (D), The ratio of mean curvature of the bend to hydraulic diameter (Rc/D) is 3.357. The curved pipe section is constructed by fitting together two symmetrical half sections of plexiglass, each respectively machined on one of the two flat faces to contain the shape of a semicircular open channel. This method of construction ensures that when matched at the common symmetry plane the cross-section of the resulting curved pipe was accurately circular.

Experiments were performed for Reynolds number similar to that of Azzola et al.(1986) (Re= 57,400). The Reynolds number is based on the bulk fluid velocity (Wb_b. The associated Dean number ($De=Re(D/Rc)^{1/2}$) is 31,300. Measurement of the mean flow and turbulent characteristics were made using a KANOMAX 7224 series hot-wire anemometer. The hot-wire probe and probe supporter were fixed with a duralumin case which was itself firmly bolted to x,y,z traversing and rotating mechanism. The traversing and rotating mechanism could displaced the hot-wire probe 15.0 cm in 0.1 mm increments on the probe axis by means of four linearly encoded stepping motors monitored by a personal computer.

Following the symmetry and mass flow confirmations, all subsequent measurements were conducted at $X/D=-19$, -5, -1, $+1$, $+6$, $+16$ in the straight pipes and $\theta=0$, 22.5, 45, 67.5, 90, 112.5, 135, 157.5 and 180 degree in the bend (Fig. 1). Scans were made at the surface at $\varphi=0$, $\pi/8$, $\pi/4$, $3\pi/8$ and $\pi/2$ (Fig. 2). At each of these stations 21 (or 11) radial positions were probed, starting at the first position fixed at 4.45 mm from the outside pipe wall ($r/(D/2)=1$) and moving in increments of 4.0 mm toward the opposite wall ($r/(D/2)=-1$).

Fig. 2 illustrates the layout of the domain of interest of the curved pipe as well as that of the coordinate system. Upstream and downstream tangents are of length $X=48.2D$ and $24D$, being, respectively, attached to 0 deg (inlet) and 180 deg (outlet) planes of the bend by means of flanges.

2.2 Measurement of mean velocity components

If we rotate the S-type hot-wire, which is inclined 45° from the Y-Z plane as shown in Fig. 3, θ degree from the reference position, the coordinate of the point A would be

$$\left(-\frac{1}{2}\cos 45^\circ \sin\theta,\ -\frac{1}{2}\cos 45^\circ,\ \frac{1}{2}\cos 45^\circ \sin\theta\right).$$

Denoting the resultant velocity vector by

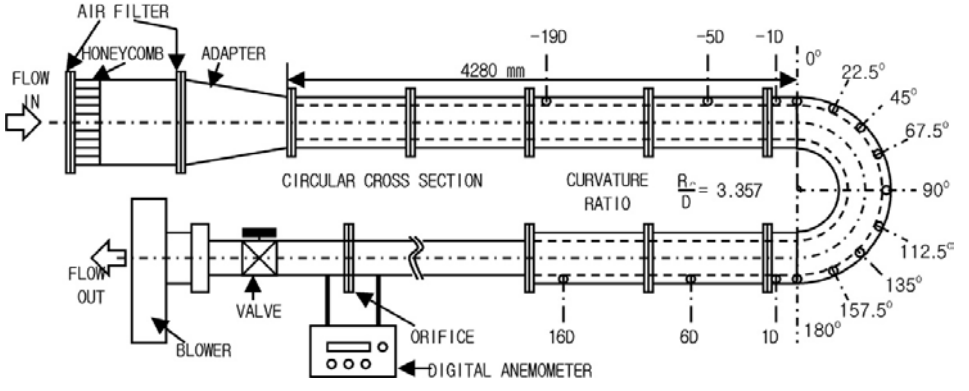

Fig. 1 Schematic diagram of experimental apparatus

$$\boldsymbol{V}_\lambda = U\mathbf{i} + V\mathbf{j} + W\mathbf{k}, \tag{4}$$

the angle ξ between resultant velocity vector $\boldsymbol{V}_\lambda$ and position vector A can be obtained by the dot product of the two vectors as follows:

$$\xi = \cos^{-1}\left(\frac{W\cos\theta - V - U\sin\theta}{\sqrt{2}\,V_\lambda}\right), \tag{5}$$

where V_λ is the magnitude of the resultant velocity. If a linearized hot-wire anemometer system is used, then the measured instantaneous voltage is related to the effective velocity (U_e):

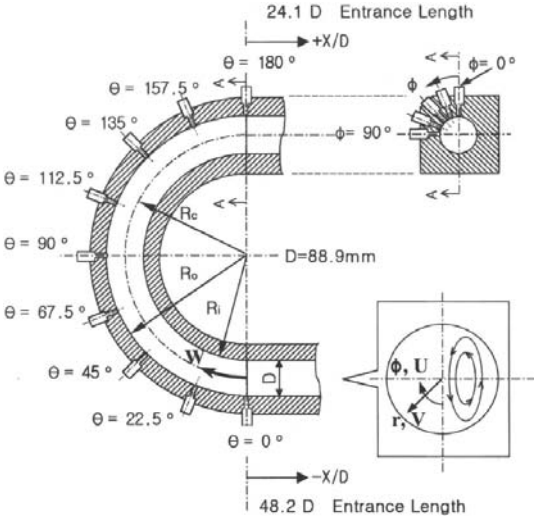

Fig. 2 The test section configuration and definition of coordinate system

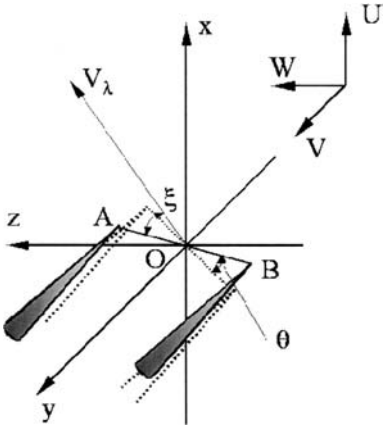

Fig. 3 Schematic diagram showing a S type wire probe rotated $\boldsymbol{\theta}$ degree from reference position

$$E_\theta = K_S U_{e\theta}, \tag{6}$$

where K_S is a proportionality constant and the subscript θ denotes the rotated angle of the probe from the reference position. Champagne (1967) suggested a relation between effective and resultant velocities,

$$U_{e\theta} = V_\lambda(\sin^2\xi + \kappa^2\cos^2\xi)^{\frac{1}{2}}, \tag{7}$$

where κ is an empirical constant. In the present study, $\kappa = 0.2$ was adopted. Substituting equations (5) and (7) into (6), one may arrive at

$$\begin{aligned} E_\theta = \frac{K_s}{\sqrt{2}}[&U^2(2-\sin^2\theta+\kappa^2\sin^2\theta) + (1+\kappa^2)V^2 \\ &+ W^2(2-\cos^2\theta+\kappa^2\cos^2\theta) + 2VW(1-\kappa^2) \\ &+ 2UW\cos\theta\sin\theta(1-\kappa^2) - 2UV\sin\theta(1-\kappa^2)]^{\frac{1}{2}}. \end{aligned} \tag{8}$$

Replacing the instantaneous values of E_θ, U, V, and W in equation (8) by their mean and fluctuating components, and expanding them in a Taylor series (neglecting terms of order higher than fifth), the following fourth order equation for the mean effective velocity $\bar{X}_\theta$ is obtained (Choi et al., 1990)):

$$3\bar{X}_\theta^4 - 8\bar{E}_\theta\bar{X}_\theta^3 + 6(\bar{E}_\theta^2 + \bar{e}_\theta^2)\bar{X}_\theta^3 - \delta_\theta = 0, \tag{9}$$

where

$$\bar{X}'_\theta = \frac{K_s\bar{X}_\theta}{\sqrt{2}} \tag{10}$$

$$\delta_\theta = \bar{E}_\theta^4 + 6\bar{e}_\theta^2\bar{E}_\theta^2 + 4\bar{e}_\theta^2\bar{E}_\theta + e_\theta^4. \tag{11}$$

where

$$\begin{aligned} &\bar{X}_\theta = (k_{\theta1}\bar{U}^2 + k_{\theta2}\bar{V}^2 + k_{\theta3}\bar{W}^2 + k_{\theta4}\bar{V}\bar{W} + k_{\theta4}\bar{U}\bar{W} + k_{\theta4}\bar{U}\bar{V})^{1/2} \\ &k_{\theta1} = 2-\sin^2\theta+\kappa^2\sin^2\theta \\ &k_{\theta2} = 1+\kappa^2 \\ &k_{\theta3} = 2-\cos^2\theta+\kappa^2\cos^2\theta \\ &k_{\theta4} = 2(1-\kappa^2) \\ &k_{\theta5} = 2\cos\theta\sin\theta(1-\kappa^2) \\ &k_{\theta6} = 2\sin\theta(1-\kappa^2). \end{aligned}$$

If $\bar{E}_\theta$, $\bar{e}_\theta^2$, $\bar{e}_\theta^3$, $\bar{e}_\theta^4$ are measured for each probe angle, $\bar{X}_\theta$ can be calculated from equation (9) by rotating the S-type probe into $\theta = 60°$, $90°$, $120°$ and $270°$, and followed by the I-type probe into $60°$, $120°$. $\bar{E}_\theta$, $\bar{e}_\theta^2$, $\bar{e}_\theta^3$, $\bar{e}_\theta^4$ were measured for each angle. If the positive roots of equation (9) for the

corresponding probe angles are denoted by X_1'', X_2'', X_3'', X_4'', X_5'', and X_1'', many sets of simultaneous equations for $\bar{U}$, $\bar{V}$, and $\bar{W}$ can be obtained from equation (8). Among the sets of equations, we can choose the optimal relation that can give minimum uncertainty of the mean velocity calculation due to its diagonal dominance of the solution matrix. The resulting relations are written as

$$\bar{U}=[(\bar{X}_5'')^2-(\bar{X}_6'')^2]/[\sqrt{3}K_s^2(1-\kappa^2)\bar{W}] \quad (12)$$

$$\bar{V}=[2(\bar{X}_1'')^2-2(\bar{X}_2'')^2-(\bar{X}_5'')^2+(\bar{X}_6'')^2]/[2K_s^2(1-\kappa^2)\bar{W}] \quad (13)$$

$$\bar{W}=[(\bar{X}_3'')^2+(\bar{X}_4'')^2+(1+\kappa^2)(\bar{U}^2+\bar{V}^2)]^{\frac{1}{2}}. \quad (14)$$

2.3 Measurement of reynolds stress components

In the present study, the Janjua et al's.(1982) correlation was used to calculate the Reynolds stress components. The tensor form for the correlation is

$$\begin{aligned}\bar{u}_i\bar{u}_m=&\sum_{i=1}^{6}\frac{\partial\bar{U}_l}{\partial\bar{E}_i}\frac{\partial\bar{U}_m}{\partial\bar{E}_i}\bar{\sigma}_{E_i}^2+\sum_{i=1\neq j}^{6}\sum_{j=1}^{6}\frac{\partial\bar{U}_l}{\partial\bar{E}_l}\frac{\partial\bar{U}_m}{\partial\bar{E}_j}\bar{K}_{E_iE_j}\\&-\Big[\frac{1}{2}\sum_{i=1}^{6}\frac{\partial^2\bar{U}_l}{\partial\bar{E}_i^2}\bar{\sigma}_{E_i}^2+\sum_{i=1i<j}^{6}\sum_{j=1}^{6}\frac{\partial^2\bar{U}_l}{\partial\bar{E}_l\partial\bar{E}_j}\bar{K}_{E_iE_j}\\&\times\frac{1}{2}\sum_{i=1}^{6}\frac{\partial^2\bar{U}_l}{\partial\bar{E}_i^2}\bar{\sigma}_{E_i}^2+\sum_{i=1i<j}^{6}\sum_{i=1}^{6}\frac{\partial^2\bar{U}_m}{\partial\bar{E}_l\partial\bar{E}_j}\bar{K}_{E_iE_j}\Big],\end{aligned} \quad (15)$$

where $\bar{\sigma}_{E_i}^2$ represents $\bar{\sigma}_\theta^2$ for a given probe angle and $K_{E_iE_j}$, is the covariance between wire i and wire j.

Jackson and Lilley (1983) used the following covariance relation in their experimental work:

$$K_{E_iE_j}=\gamma_{iE_j}(\bar{\sigma}_{E_i}^2\bar{\sigma}_{E_j}^2)^{\frac{1}{2}}, \quad (16)$$

where $\gamma_{E_iE_j}$ is the correlation coefficient between wires i and j. King (1978) made a certain assumption by calculating the covariance coefficient. He argued that if two wires are separated by an angle of 30 degrees, the contribution of the correlation coefficient would be related by the cosine of the angle between the wires as follows:

$$\gamma_{E_iE_j}=\cos 30°=0.87. \quad (17)$$

When separation angle θ is a multiple of 30°, he used the following correlation coefficients:

$$\gamma_{E_iE_j}=0.8(\cos 30°)^n. \quad (18)$$

Choi et al.(1990) extended King's relation to angles θ, that are not multiples of 30°. Choi's correlation coefficient for separation angle $\theta=30n+\alpha$ is written as

$$\gamma_{E_iE_j}=0.8(\cos 30°)^n\cos\alpha. \quad (19)$$

If mean voltage $\bar{E}_\theta$, square mean fluctuating voltage component $\bar{e}_\theta^2$, and cubic mean of fluctuating voltage component $\bar{e}_\theta^3$ are measured for each probe angle, the Reynolds stress correlation equation (15) can be calculated by using correlation (19).

2.4 Data uncertainty

Various combinations of the present experimental program are tabulated in Table 1.

Uncertainty analysis was performed based on the method suggested by ASME Performance Test Codes (1987). It is assumed that the equipment has been constructed correctly and calibrated properly to eliminate fixed errors. Thus, the uncertainties of the measured quantities in the present experiments are assumed to be random with normal distribution. The uncertainty of the Reynolds number and digital manometer is estimated as 0.94% and 0.2%, and the uncertainties of hot-wire for mean and fluctuating velocities are estimated as 4.4% and 2.9%, respectively. Therefore, the combined uncertainties of pressure coefficients, and mean and fluctuating velocities are estimated as 0.96%, 4.5% and 3.0%, respectively.

Table 1 Experimental program and flow conditions

Scans in the straight pipes (X/D)	−19, −5, −1, +1, +6, +16,
Scans in the bend (θ)	0°, 22.5°, 45°, 67.5°, 90°, 112.5°, 135°, 157.5°, 180°
Scans in the cross-sections (φ)	0, $\pi/8$, $\pi/4$, $3\pi/8$, $\pi/2$,
Inter diameter	88.9 mm
Reynolds number	57,400

3. Results and Discussions

In Fig. 4, present measurements of the longitudinal (W/W_b) and circumferential (U/W_b) velocity components are compared with Azzola et al.'s (1986) experiment data along the line $\varphi=90°$ at sequential longitudinal stations in a 180 deg pipe with straight tangents. The longitudinal and circumferential mean velocity distributions along the line $\varphi=90°$ show very good agreement with Azzola et al.'s data. Over the initial part of the bend a strong secondary vortex flow develops due to the imbalance between cross-stream pressure gradient and centrifugal force. Cuming (1952) shows analytically that, for equal radius of curvature to diameter ratio and dimensionless streamwise pressure drop, the ratio of the relative intensity of the secondary flow in a duct of square cross-section to that of circular cross-section is 2.47 at the center line location. However, comparisons between the present results and corresponding measurements by Chang et al. (1983) in a curved duct of square cross-section with similar developing turbulent flow characteristics show that the secondary motion ratio can be considerably larger than 2.47. In Fig. 4, reversal of secondary flow direction is found along the bend symmetry plane between $\theta=135°$ and $X/D=5$. It is caused by the breakdown of counter-rotating vortex pair into two cellular pattern and thereby formation of secondary core vortex.

Figure 5 shows that present measurements for longitudinal and circumferential turbulent intensities are in good agreement with Azzola et al.'s data except $\theta=90°$ at which the secondary flow pattern changes rapidly. Over the initial part of bend, both (w'/W_b) and (u'/W_b) have maximum values in the wall region, but they decrease gradually away from the wall. However, after $\theta=90°$, local maximums of the turbulent intensities appear in the core region of the bend. This is

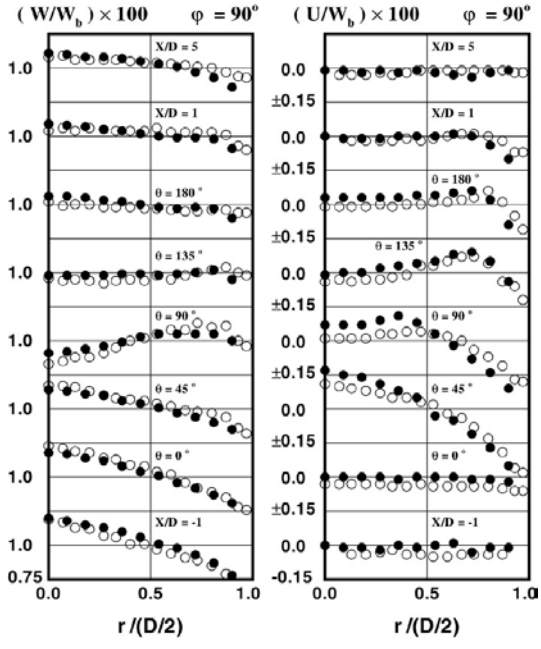

Fig. 4 Comparisons of the measured longitudinal (W/W_b) and circumferential (U/W_b) mean velocity components at sequential longitudinal stations in a 180 deg curved pipe with straight tangents; ● : present data, ○ : Azzola et al. (1986)

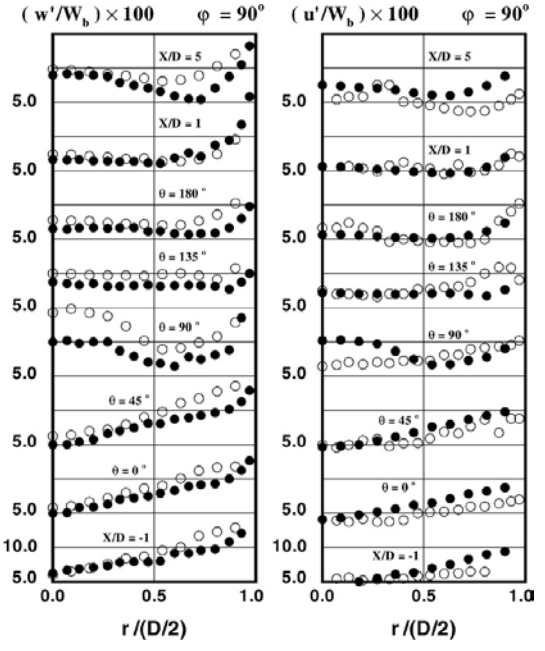

Fig. 5 Comparisons of the measured longitudinal (w'/W_b) and circumferential (u'/W_b) turbulence intensities at sequential longitudinal stations in a 180 deg curved pipe with straight tangents; ● : present data, ○ : Azzola et al. (1986)

caused by the breakdown of counter-rotating vortex into two cellular pattern.

In the present measurements, (w'/W_b) have a little larger values than (u'/W_b), but the distributions show nearly same shapes in the whole region. At the station $\theta=90°$, however, Azzola et al.'s (w'/W_b) distribution shows too different trend from that of (u'/W_b). Therefore, we expect the possibility of measurement error for the Azzola et al.'s data at the station $\theta=90°$.

Figure 6 shows the variation of the longitudinal velocity in the sequential cross-sectional planes from the inlet to the outlet of the bend. At the bend entrance $(\theta=0°)$, W velocity profile of present measurement shows different shapes with that of the fully developed flow. Scans made at $X/D=-19$ in the upstream tangent show the W velocity profile of the fully developed flow measured by Laufer (1954) in a straight pipe. Some asymmetry in W velocity profile is found at $\theta=0°$. As shown in Fig. 6, from the inlet of the straight pipe to the entrance region of the bend, the flow is gradually accelerated in the inner wall region of the bend $(r/(D/2)<0)$ while de-

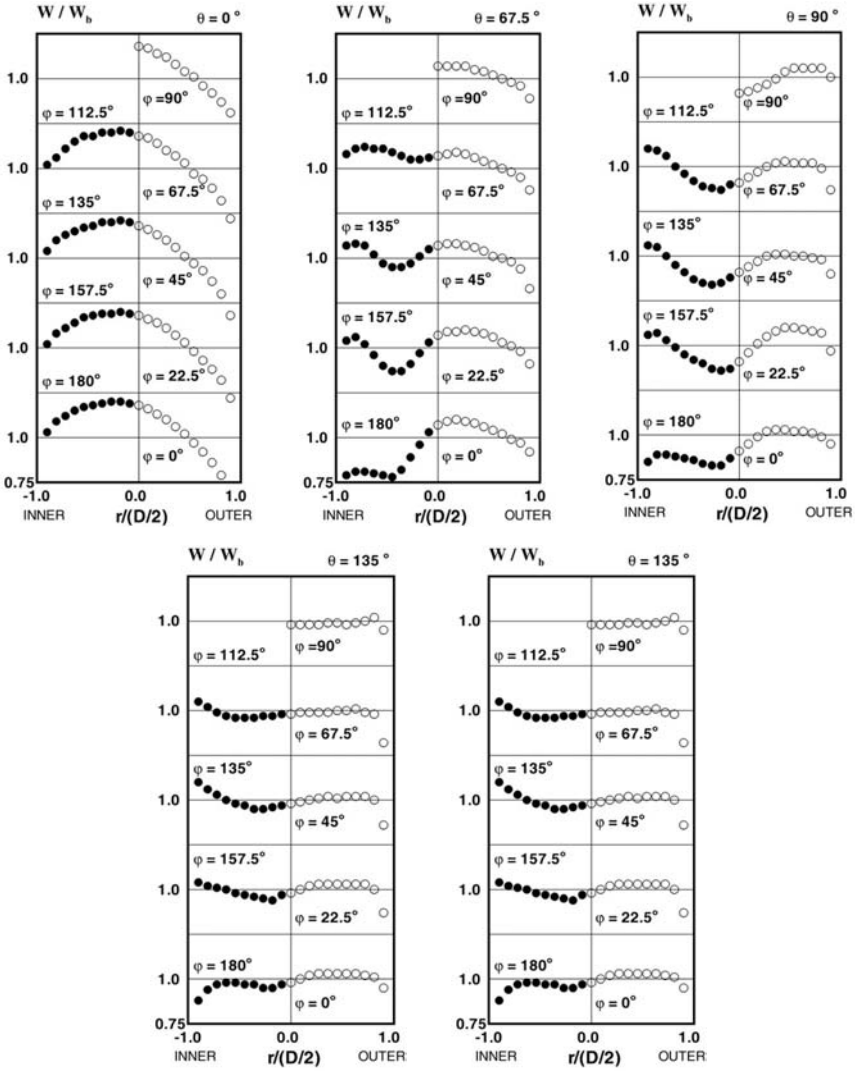

Fig. 6 Distribution of the longitudinal mean velocity component at sequential longitudinal stations in a 180 deg curved pipe with straight tangents

celerated in the outer wall region ($r/(D/2)>0$). Low pressure of inside region of the bend in the entrance region accelerates the longitudinal velocity component and high pressure of the outer region of the bend decelerates the longitudinal velocity in that region. At $\theta=67.5°$ and $\theta=90°$ into the bend a large "trough" develops in the longitudinal velocity toward the inside of the bend. The most interesting feature of the 180° bend flows is the development of a large trough and thus of double peaks in the longitudinal velocity profiles (Chang et al., 1983; Choi et al., 1989; Azzola et al., 1986). Over the initial part of the bend the conventional single secondary vortex carries near-wall fluid to the inside of the bend. Due to this accumulation, slow-moving fluid near the symmetry plane is pushed away from the inside wall towards the outside of the bend. However, because its longitudinal velocity is low it cannot proceed far against the radial pressure gradient; the fluid is deflected at roughly right angles to the symmetry plane and then turns back on itself towards the inside of the bend. Thus, interaction of primary and secondary flow leads to a progressive vortex breakdown. The troughs in longitudinal velocity near the inside of the bend at $\theta=67.5°$ and $\theta=90°$ in Fig. 6 are obviously formed by this breakdown of secondary flow.

A more complete picture of the developing secondary flow through the bend is provided in Fig. 7

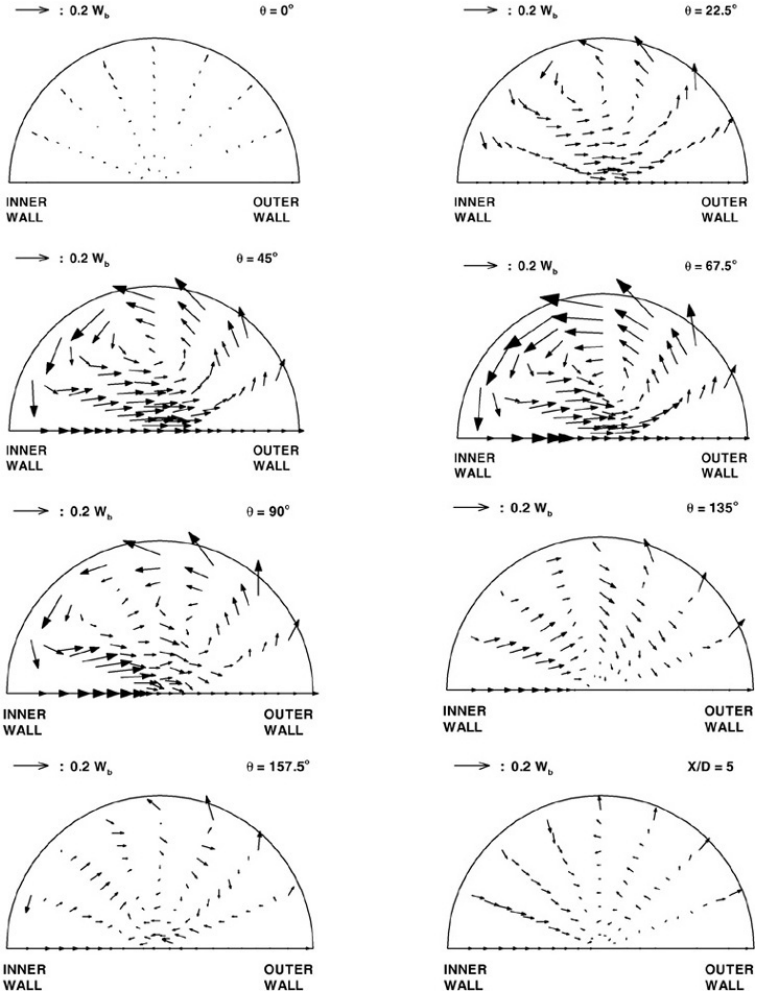

Fig. 7 Vector plot for the secondary flow development in a 180 deg curved pipe with straight tangents

which shows the secondary vectors. A strong cross-stream motion induced by the transverse pressure gradient and centrifugal force imbalance grows up to $\theta=67.5°$ forming a counter-rotating vortex pair. In the Rowe's experiment, the most intense secondary flow was found at $\theta=30°$, but at $\theta=67.5°$ in the present experiment. This may be due to the difference in Dean numbers of the two flows, being De=68,000 in Rowe's bend and 31,300 in the present bend. At $\theta=67.5°$, the secondary flow intensity $((U^2+V^2)^{1/2}/W_b)$ near the wall increases up to 0.28. However, in the last half of the bend ($\theta=90°$ to 180°), the secondary vortex gradually decays and breakdowns into two cellular pattern. Breakdown of core vortex from primary vortex and consequent reversal of secondary flow direction along the symmetry plane is found at $\theta=135°$ and $\theta=157.5°$.

Choi et al.(1997) reported fine grid calculations for the same flow condition with Azzola et al.'s (1984) experiment using both k-ε eddy viscosity model and algebraic second moment closure. In the Choi et al.'s computational results, a large core vortex is formed at $\theta=135°$. The core

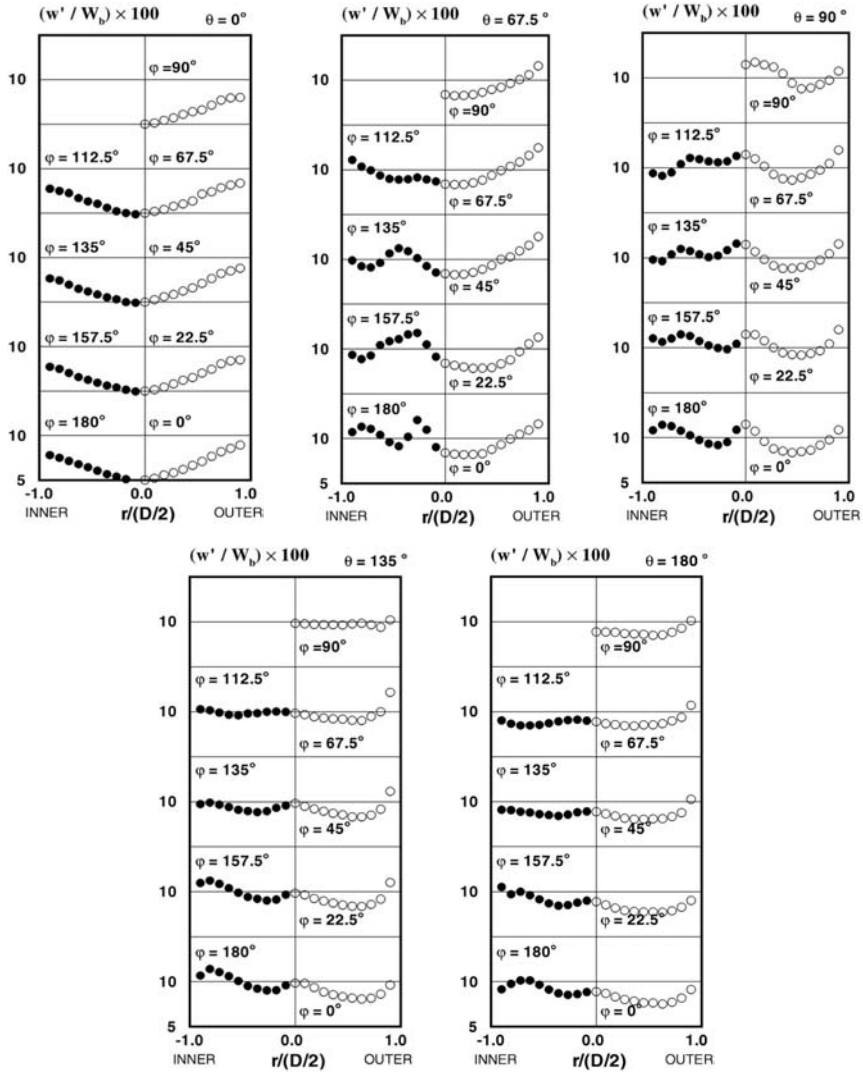

Fig. 8 Distribution of the longitudinal turbulent velocity component at sequential longitudinal stations in a 180 deg curved pipe with straight tangents

vortex center is located at $r/R=0.306$ and $\varphi=90°$ for the simulation by k-ε eddy viscosity model and at $r/R=0.286$ and $\varphi=80°$ for the simulation by second moment closure. In the secondary vectors in Fig. 7, the core vortex center is located at $r/R=0.287$ and $\varphi=110°$. Regarding to r/R, Choi et al's second moment closure predicts the core vortex center close to the present experimental data. On the other hand, regarding to φ, k-ε eddy viscosity model shows better result.

Figure 8 shows the variation of longitudinal turbulent intensity in the sequential cross-sectional planes from the inlet to the outlet of the bend. At the bend entrance ($\theta=0°$), w'/W_b profiles from the present measurement shows nearly the same shape with that of fully developed profiles of a straight pipe. However, in the entrance region, from $\theta=0°$ to $\theta=90°$, w'/W_b increases rapidly according to the development of counter-rotating vortex. As with the decrease in counter-rotating vortex in the second half of the bend, w'/W_b gradually decreases. Additional mean strain associated with the distorted stream-wise velocity profiles in the inside region of the bend at $\theta=67.5°$ and $\theta=90°$ induces the distortion of w'/W_b in those regions. The propagation of turbulence generated in the inner wall region of the bend toward the core of the bend is also shown in Fig. 8. But it does not propagate over $r/(D/2)>0$. Streamline curvature can affect turbulent structures in the curved duct or pipe flows. However, any evidence of the effect on turbulence structure can not be found in the Fig. 8. In the curved duct or pipe flows, production of turbulence by secondary flow predominates that by streamline curvature.

Full mapping of circumferential turbulent intensity and Reynolds shear stress distributions at the station of $\theta=67.5°$ are shown in Fig. 9. The distributions of u'/W_b shown in Fig. 9 give nearly the same shapes as those of w'/W_b in Fig. 8 while having relatively small values. All the turbulent intensities and Reynolds shear stress components in the inside region of the bend show highly curved at $\theta=67.5°$ effect of mean velocity distortions. Magnitudes of $\overline{vw}/W_b^2$ and $\overline{uv}/W_b^2$ distributions are relatively smaller than those of $\overline{uw}/W_b^2$.

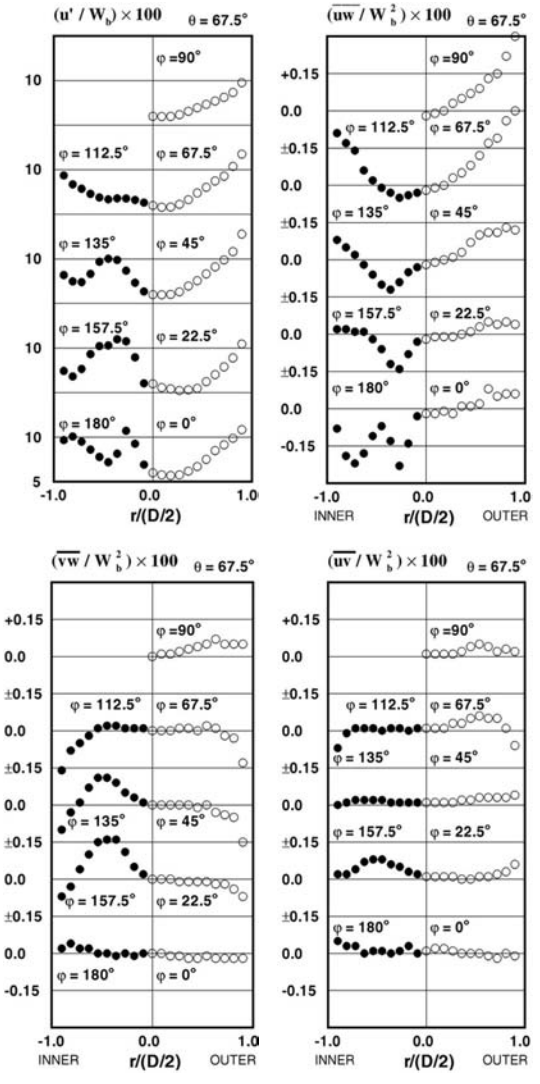

Fig. 9 Distributions of circumferential turbulent intensity and Reynolds shear stress components at $\theta=67.5°$ in a 180 deg curved pipe with straight tangents

4. Conclusions

In the present paper a complete mapping of turbulent flow characteristics in a 180 deg bend of circular cross-section is reported for the conditions corresponding to those for which Azzola et al. provided detailed data. The following conclusions are obtained

(1) The present measurements for longitudinal and circumferential mean velocities and tur-

bulent intensities along the line $\varphi=90°$ give very good agreement with Azzola et al.'s LDV measurement. However, at $\theta=90°$ where the cross-stream motion changes the most rapidly, significant difference is found in turbulent intensities at $\theta=90°$.

(2) The W velocity profiles along the radial lines give double peaks after $\theta=90°$ due to the breakdown of secondary flow field into two cellular pattern.

(3) The level of the measured secondary flow intensity in the present measurement is lower than that of the 180° curved duct of a square cross-section.

(4) In the entrance region of the bend, Reynolds stress productions are highly enhanced by the secondary vortex. Additively generated Reynolds stresses in the inner wall region near symmetry plane in the first half of the bend propagates toward the core of the bend.

(5) The present study provides a full mapping for the distributions of the longitudinal and circumferential mean velocities and all the Reynolds stress components over the 180° curved pipe and its tangents.

These results would help workers who want to develop the more reliable turbulent models for the CFD analysis of three dimensional turbulent flows.

Acknowledgments

The paper was supported by Wonkwang and Korea Universities in 1998.

References

Azzola, J., Humphrey, J. A. C., Iacovides, H. and Launder, B. E., 1986, "Developing Turbulent Flow in a U-bend of Circular Cross Section : Measurement and Compu tation," *J. Fluid Eng.*, Vol. 108, pp. 214～221.

Champagne, F. H., Sleicher, C. A. and Wehrmann, O. H., 1967, "Turbulence Measurements with Inclined Hot-Wire," *J. Fluid Mech.*, Vol. 28, part 1, pp. 153～175.

Chang, S. M., Humphrey, J.A.C. and Modavi, A., 1983, "Turbulent Flow in a Strongly Curved U-Bend and Downstream Tangent of Square Cross-Sections," PysicoChemical hydrodynamics, Vol. 4, No. 3, pp. 243～269.

Choi, Y. D., Iacovides, H. and Launder, B. E., 1989, "Numerical Computation of Turbulent Flow in a Square-Sectioned 180 Deg Bend," Transaction of ASME, J. of Fluids Engineering, Vol. 111, pp. 59～68.

Choi, Y. D., Kim, S. S. and Humphrey, J. A. C., 1997, "Modeling Turbulent Flow in a 180° Bend of Circular Cross Section," Transport Phenomena in Thermal Science and Process Engineering, Koyto, Japan : November 30-December 3, pp. 127～132.

Choi, Y. D., Moon, C. and Yang, S. H., S. H., 1990, "Measurement of Turbulent Flow Characteristics of Square Duct with a 180 Degree Bend by Hot-Wire Anemometer," *Proc. of the International Symposium on Turbulence Modeling and Experiments*, Dubrovnik, pp. 429～438.

Choi, Y. D., Shin, J. K., Chun, K. H. and Humphrey, J. A. C., 1997, "Modeling Turbulent Flow in a Curved Duct of Square Cross-Section," *Proc. of 11th Symposium on Turbulent Shear Flows*, Grenoble, France, pp. 3.47～3.52.

Cumming, H. G., "The Secondary Flow in Curved Pipes," NPL, UK, Reports and Memoranda, No. 2880, Feb. 1952.

Dean, W. R., 1927, "Note on the Motion of Fluid in a Curved Pipe," *Philos. Mag.*, Vol. 20, pp. 208～223.

Dean, W. R., 1928, "The Streamline Motion of Fluid in a Curved Pipe," *Philos. Mag.*, Vol. 30, pp. 673～693.

Humphrey, J. A. C., Whitelaw, J. H. and Yee, G., 1981, "Turbulent Flow in a Square duct with Strong Curvature," *J. Fluid Mech.*, Vol. 103.

Jackson, T. W. and Lilly, D. G., 1983, "Single Wire Swirl Flow Turbulence Measurement," AIAA 83-1202, Cleveland, Ohio.

Janjua, S. I., Mclaug, D. K., Jackson, T. W. and Lilly, D. G., 1982, "Turbulence Measurements in a Confined Jet Using a Six-Orientation Hot-Wire Probe Technique," *AIAA 82-1262*, Cleveland, Ohio.

King, C.F., 1978, Ph.D. Thesis, Univ. College of Wales, Cardiff, Wales.

Rowe, M., 1970, "Measurement and Computations of Flow in Pipe Bends," *J. Fluid Mech.*, Vol. 43, pp. 771～783.

Taylor, A. M. K. P., Whitelaw, J. H. and Yianneskis, M., 1982, "Curved Ducts with Strong Secondary Motion ; Velocity Measurement of Developing Laminar and Turbulent Flow," ASME Journal of Fluid Engineering, Vol. 104, pp. 350～359.